A DFT study of epoxidation of propylene on dimer MoO_x

Jiahui Peng[1,2] | Zhehong Wan[1,2] | Wei Chen[3] | Hui Hu[1,2] | Qingming Huang[4] | Xiaohui Chen[1,2,*]

[1] College of Chemical Engineering, Fuzhou University, Fuzhou, Fujian, China

[2] National Engineering Research Center of Chemical Fertilizer Catalyst, Fuzhou University, Fuzhou, Fujian, China

[3] State Key Laboratory of Magnetic Resonance and Atomic and Molecular Physics, National Center for Magnetic Resonance in Wuhan, Key Laboratory of Magnetic Resonance in Biological Systems, Wuhan Institute of Physics and Mathematics, Innovation Academy for Precision Measurement Science and Technology, Chinese Academy of Sciences, Wuhan, China

[4] Test center of Fuzhou University, Fuzhou University, Fuzhou, Fujian, China

Correspondence

Xiaohui Chen, College of Chemical Engineering, Fuzhou University, Fuzhou

350116, Fujian, China.

Email: chenxhfzu@fzu.edu.cn

Funding information

National Natural Science Foundation of China, Grant/Award Number: 21571036

Abstract

Propylene oxide is an important chemical raw material. In this paper, Density Functional Theory (DFT) was used to calculate the epoxidation of propylene on the dimer MoO_x by Gaussian 09 software. Firstly, we established the structure of the dimer MoO_x/SiO_2 and analyzed it, and then calculated the dehydrogenation process of propylene and the formation process of PO. It was found that the activity of O in Mo-O-Si was higher, which was beneficial to the AHS process of C_3H_6, but the reaction activity of different O substances to the formation of PO was very low. In order to solve this problem, we established a dimer MoO_x model with defect sites, and found that the defect sites in the dimer could effectively activate O_2 (O_2^{2-}), and the activated material O had high PO selectivity. Compared with process of AHS and the process of PO formation, the energy barrier of PO formation path was very low, which was the main product. At the same time, we also established the MoO_x model of Fe doped dimer and the MoO_x model of Fe doped defect dimer. It was found that the MoO_x clusters were more active due to Fe doping, and the energy barriers of both AHS process and PO formation path were greatly reduced compared with those before doping. The presence of Fe made it easier for the dimer MoO_x to form defect sites, which made it easier to activate O_2 (O_2^-) and reduced the energy barriers of both AHS and PO formation processes.

KEYWORDS

propylene epoxidation, DFT, dimer MoO_x, defect, doping

1 | Introduction

Propylene oxide is an important chemical product, which plays an important role in the chemical industry. Propylene oxide is the third largest propylene derivative after polypropylene and acrylonitrile. At present, propylene oxide is mainly made from propylene in industry. The main synthesis methods are [1]: chlorohydrin method, co-oxidation method (PO/SM, PO/TBA), hydrogen peroxide method, oxidation method of isopropylbenzene and direct gas phase oxidation (C_3H_6, O_2 or N_2O). Among these catalysts, the selective oxidation of hydrocarbons over Mo based catalysts has always been an important topic [2-5] .

Previous studies found that Mo-Bi catalyst system had high selectivity and propylene conversion for partial oxidation of propylene to acrolein, and the main active material was $Bi_2Mo_3O_{12}$. Therefore, many researchers have carried out theoretical research on the reaction of MoO_3 [6, 7], and the research on Mo-Bi system catalyst for acrolein has reached the industrial standard and has been put into commercial application. Mimura and others [8, 9] reported that MoO_3/SiO_2 catalyst had excellent performance in propylene epoxidation, with propylene conversion of 17.6%. The selectivity of PO was 43.6% (reaction conditions: pressure 5 atm, temperature 300 °C, feed $C_3H_6/O_2/He$ = 10/5/10 $cm^3 \cdot min^{-1}$), indicating that the crystalline MoO_3 may be more active than monodisperse Mo. They also studied the epoxidation of propylene using different supports such as MgO、ZrO_2、α-Al_2O_3、γ-Al_2O_3 and SiO_2, but using the same method to support MoO_x. The results showed that different supports had an important influence on the catalytic reaction. For example, MoO_x/MgO mainly formed CO_x. Compared with other supports, MoO_x supported by ZrO_2、α-Al_2O_3、γ-Al_2O_3 and SiO_2 was more favorable. These carriers had higher activity.

Horváth et al.[10] prepared the catalysts with different precursors and different methods, and found that the selectivity of crystalline MoO_3 to PO was very low, while the selectivity of amorphous octahedral Mo species anchored on the support was 55%, and the conversion of C_3H_6 was 11%. Therefore, MoO_x catalyst has great potential for the epoxidation of C_3H_6. But at present, the research on the structure of MoO_x and partial oxidation of propylene mainly focuses on the crystal α-MoO_x or its simplified configuration. The structure of α-MoO_x is shown in Figure 1. The interaction between atoms in the layer is strong ionic bond and covalent bond, while the interaction between layers is weak Van Der Waals force, which is a distorted octahedral structure. However, there are few studies on the mechanism of partial oxidation of propylene on MoO_x.

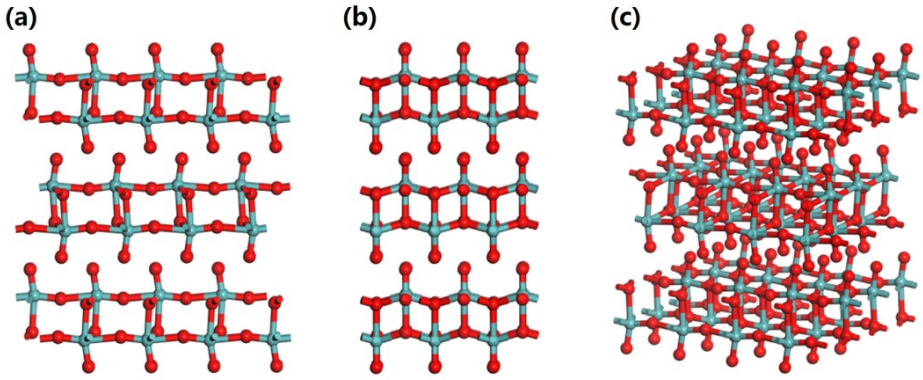

FIGURE 1 Schematic diagram of the crystal α-MoO_x: (a) front view, (b) left view and (c) side view.

Later, Wan et al.[11] studied the epoxidation process of propylene on MoO_x by density functional theory, and further studied the gas phase epoxidation mechanism of propylene. The results showed that gas phase free radical reactions have important effects on PO generation, in which $C_3H_5OO•$ is the main active species and on MoO_x surface, Mo=O is difficult to be used as the active O species for PO production.

In view of the excellent catalytic effect of Mo based catalysts, therefore, combined with the previous research experience, we chose the amorphous MoO_x structure with strong interaction with the support SiO_2. So, we first calculated the structure of dimer MoO_x and the propylene epoxidation reaction on it, and calculated the model of Fe doped dimer MoO_x, and the influence of these two models on the reaction when there are defect sites.

We used Gaussian 09 software in this simulation. In the calculation configuration, 6-31g(d, p) [12, 13]basis group was used for C, H, O and Si, Mo and Fe were geometrically optimized by using B3LYP/Lanl2DZ[14-17] named pseudo potential basis group, while the energy calculation was used to describe C, H, O, Si, Mo and Fe at a higher level, which we used B3LYP/6-311+G(d, P)[18-22], Lanl2DZ[17, 23]. B3LYP/Lanl2TZ was used to calculated Mo and Fe, and DFT-D3 was added for dispersion correction. Because of the special electron configuration of Fe element, the spin weight of the whole Fe-doped MoO_x cluster is 6 when it is the most stable.

2 | Partial oxidation mechanism of propylene on MoO_x/SiO_2 dimer

2.1 | Dehydrogenation mechanism

Figure 2 shows the AHS process on different O substances, which has similar dehydrogenation process on different O substances.

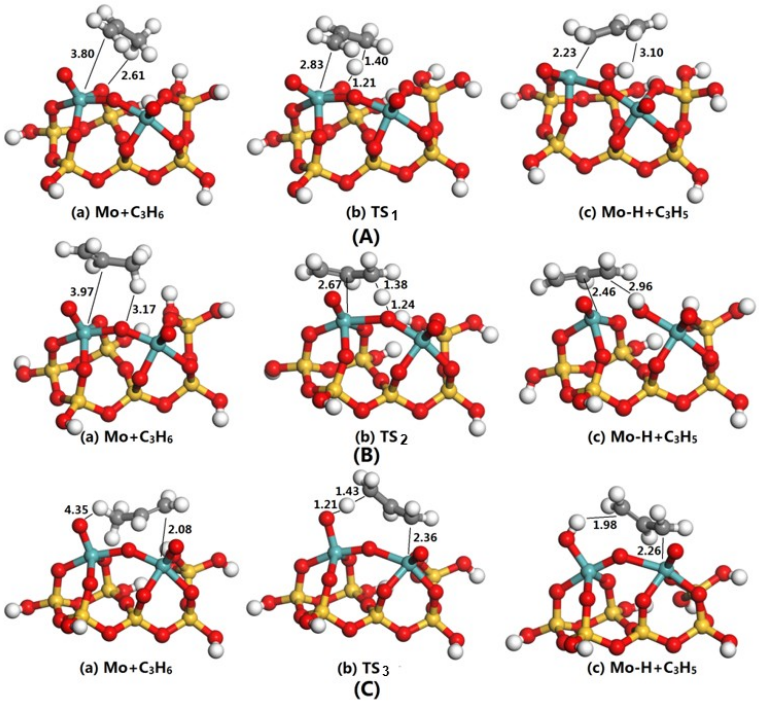

FIGURE 2 Dehydrogenation paths on different O species in MoO*x*: (A) Mo-O-Si, (B) Mo-O-Mo, (C) Mo=O

First of all, the physically adsorbed C_3H_6 forms -OH and C_3H_5 through the transition state. In the AHS process, the α-H of C3 gradually tends to the lattice O. At the same time, due to the coordination between the lattice O and H, the distance between the lattice O and Mo center becomes longer, and the dehydrogenated C_3H_5 will form a coordination bond with the nearby Mo center. This process makes the generated C_3H_5 easily form a strong interaction with MoO_x, it is difficult to desorb. Figure 2 and Figure 4 show the reaction path and energy diagram of different processes respectively. It can be seen that under the action of O in Mo-O-Si, the process of forming Si-OH and C_3H_5 needs to span 28.89 kcal/mol energy, and the desorption of C_3H_5 needs to absorb 9.17 kcal/mol energy. However, Mo-OH and C_3H_5 are formed in the AHS process when O acts in Mo-O-Mo, and the energy barrier of the whole process is 37.82 kcal/mol. C_3H_5 needs to absorb 3.92 kcal/mol energy to desorption. Moreover, for Mo=O, the energy barrier of AHS process needs to cross a higher barrier (45.85 kcal/mol), and the desorption of C_3H_5 needs 7.38 kcal/mol energy.

The results show that the O in Mo-O-Si is more conducive to dehydrogenation than the O in Mo-O-Si. This is consistent with the analysis results of HOMO-LUMO, which further confirms that the O material in Mo-O-Si is more active, but compared with the results of monomer four coordination MoO_x[11], $Mo(=O)_2$ has higher dehydrogenation.

2.2 | Formation mechanism of PO

The path of PO formation on different O substances is shown in Figure 3. The reaction path is similar to that of metal oxides. There are two main reaction sroutes, one is through the intermediate of OMP (metal-oxygen heterocyclic intermediate), the other is direct oxidation.

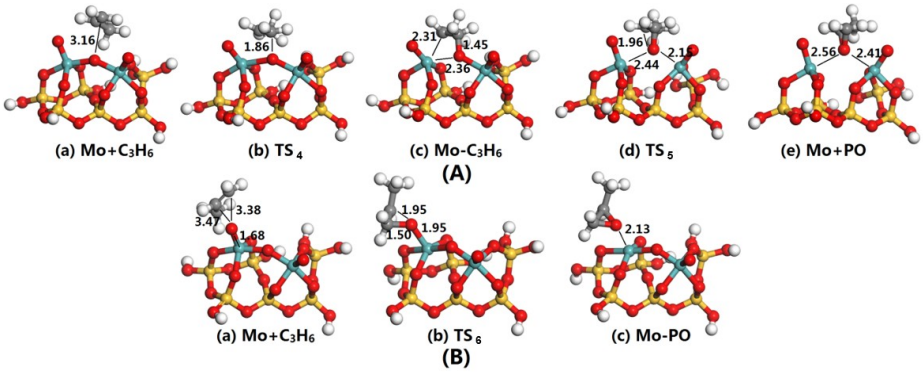

FIGURE 3 The paths of PO generation on different O species in MoO_x: (A) Mo-O-Mo, (B) Mo=O

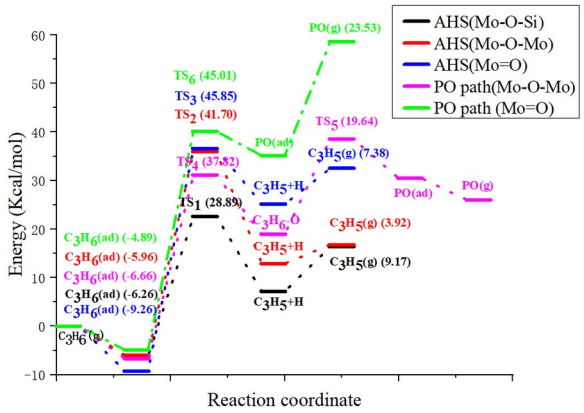

FIGURE 4 Energy profile of different reaction paths of C_3H_6 on MoO_x

The epoxidation of propylene on Mo-O-Mo is mainly through the intermediate of OMP to form PO. Firstly, C_3H_6 in the form of physical adsorption passes through the transition state TS_4. In this process, the distance between C1 and O in Mo-O-Mo is shortened from 3.16 Å to 1.86 Å, and with the stretching of Mo1-O bond length in Mo1-O-Mo2, OMP intermediate is formed, in which the C1-O bond length is 1.45 Å, the coordination length between C2 and Mo center is 2.31 Å, and Mo1-O is pulled up to 2.36 Å. The energy barrier of this process is 37.82 kcal/mol. After that, the intermediate was closed-loop -C1-O-C2-, and PO is formed through transition state TS_5. This process is accompanied by the gradual separation of O from Mo1-O-Mo2, the distance from Mo1 and Mo2 becomes longer, and the energy barrier is 19.64 kcal/mol. During the whole process, the formation of OMP intermediate is a rate control step.

The mechanism of epoxidation on Mo=O is direct oxidation. PO is produced by directly pulling O from Mo=O without intermediate state. The distances between C1, C2 and O (Mo=O) in physically adsorbed C_3H_6 are 3.38 Å and 3.47 Å respectively. After the transition state TS_6, C1 and O are bonded, the bond length is 1.50 Å, the distance between C2 and O is 1.95 Å, and -C1-O-C2- is cyclized to form PO. The energy barrier of this process is as high as 45.01 kcal/mol. As for the formation mechanism of PO on Mo-O-Si, due to the strong bond and interaction between Si-O, the connected O is difficult to be pulled out, and this process is difficult to achieve, so it is not detailed here.

Through the analysis of the two kinds of epoxidation mechanism, it can be seen that in different O substances on the dimer, the mechanism path of PO formation by OMP intermediate or direct epoxidation needs to cross a higher energy

barrier, reaching 37.82 kcal/mol and 45.01 kcal/mol respectively. Compared with the AHS process on Mo-O-Si (energy barrier 28.89 kcal/mol), the PO formation path is not a favorable one. Therefore, there is no further study on the pathway from OMP intermediate to by-product propionaldehyde and acetone.

3 | Dehydrogenation of C_3H_6 at defect sites of MoO_x/SiO_2 dimer and formation mechanism of PO

It can be seen from the previous studies that the O^{2-} in the MoO_x/SiO_2 structure of the catalyst, whether Mo=O or Mo-O-Mo, is difficult to improve the selectivity of PO. In order to further understand the main active sites of MoO_x/SiO_2, this section mainly explores the role of defect sites on the catalyst, and explores the reaction mechanism on it.

3.1 | Formation and properties of O-defect sites in MoO_x

For the complete coordinative MoO_x structure, it is difficult to activate O_2 due to the space effect, and the formation of defect sites will lead to the exposure of central metal atoms and easy to contact with other reactive molecules.The structure of O-defect site of dimer MoO_x is shown in Figure 5.

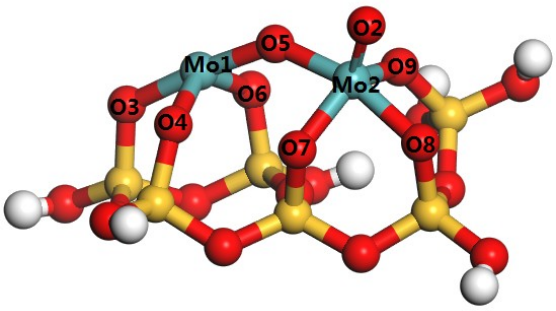

FIGURE 5 MoO_x cluster structure with an O-defect site

The formation energy of defect sites in the structure can be calculated by the following formula:

$$\Delta E_O = E_{defect\ site} + 1/2 E_{O_2} - E_{total} \quad (1)$$

Where ΔE_O is the formation energy of O defect site, E_{total} is the total energy of complete cluster structure, $E_{defect\ site}$ is the energy of cluster structure with defect site, and E_{O_2} is the energy of one O_2, the unit is kcal/mol. According to the calculation, the formation of defect site of dimer MoO_x configuration is 100.10 kcal/mol.

3.2 | Partial oxidation of propylene at defect sites

In order to further understand the partial oxidation reaction of C_3H_6 at the defect site, we calculated the different reaction paths of C_3H_6, as shown in Figure 6, mainly involving the AHS process and PO generation path, and the energy path is shown in Figure 7.

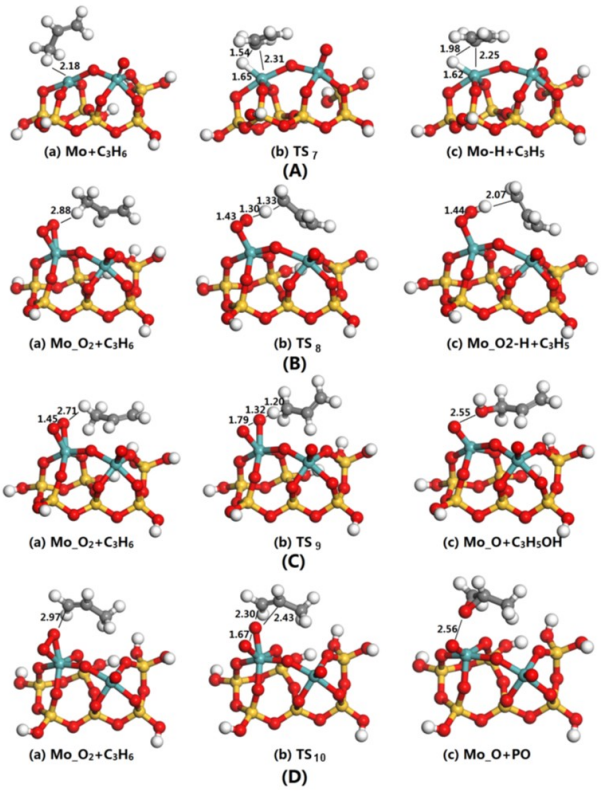

FIGURE 6 Schematic diagram of different paths of C_3H_6 at MoO_x defect sites. (A) The AHS process at defect sites, (B) (C) (D) AHS, C_3H_5OH and PO generation paths on are activated O_2

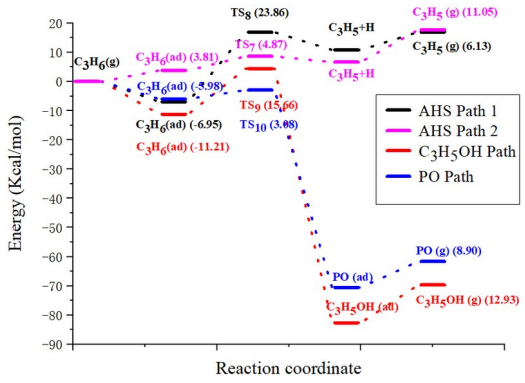

FIGURE 7 Energy profile of different paths of C_3H_6 at MoO_x defect site

Figure 6 (A) shows the AHS process on the defect site, which is the removal of α-H with the defect site as the main active center. The surrounding C_3H_6 interacts with Mo to form Mo-H and C_3H_5 through transition state TS_7. From the beginning to the transition state of TS_7, the distance between Mo and H changes from 2.18 Å to 1.65 Å, and the bond length of C3-H changes from 1.10 Å to 1.54 Å. Therefore, the desorption of C_3H_5 is a rate control step in the whole process. However, it should be made clear that in this initial process, the adsorption state of C_3H_6 is not stable, which is 3.81 kcal/mol of heat absorption. Compared with the stable adsorption state of C_3H_6 exothermic -32.45 kcal/mol, this state is not favorable.

Figure 6 (B) (C) (D) shows the interaction between activated O_2 and C_3H_6 at the defect site, respectively. The AHS

process of C_3H_6 is shown in Figure 6 (B). The heat release of C_3H_6 in the initial physical adsorption state is about -6.95 kcal/mol, and then to the transition state TS_8. The distance between O in activated O_2 and α-H is shortened from 2.88 Å to 1.30 Å. At the same time, the bond length of C3-H is broken and the bond length is stretched from 1.10 to 1.33. Finally, Mo-OOH and C_3H_5 were generated. The energy barrier of this process is 23.86 kcal/mol, which is a rate control step. Compared with Figure 6 (B), the initial configuration of C_3H_6 in Figure 6 (C) is different, and the path of C_3H_6 in the dehydrogenation process is also different. The results show that the α-H of C_3H_6 interacts with the activated O_2. After the transition state TS_9, in addition to the C3-H bond is gradually stretched until fracture, the distance between O in the activated O_2 and H is shortened, the bond length of the activated O-O is also gradually stretched, resulting in the fracture of O-O bond and the formation of C_3H_5OH. The energy barrier of this process is 15.66 kcal/mol, which is more favorable than the simple AHS process.

As for the epoxidation activity of activated O_2 at the defect site, the path is shown in Figure 6 (D), which is a direct oxidation path without passing through OMP. The physically adsorbed C_3H_6 is directly pulled to activate one O in O_2 through the transition state. In the transition state TS_{10} configuration, the distances between O and C1 and C2 are 2.30 Å and 2.43 Å respectively, and the breaking distance of O-O bond is 1.67 Å. Finally -C2-O-C1 is cyclized to form PO. The energy barrier of this process is only 3.08 kcal/mol. However, the energy consumption of PO desorption is higher, which is 8.90 kcal/mol, which becomes the rate control step.

By comparing the different reaction paths of C_3H_6 on the defect site, it can be seen that compared with the high energy barrier of AHS process (23.86 kcal/mol) and C_3H_5OH formation path (15.66 kcal/mol), the formation path of PO is the most favorable, and the highest energy barrier to be crossed is only 8.90 kcal/mol, and the whole process is a strong exothermic process. It can be seen that PO is the main product on the MoO_x cluster with defect sites and has high selectivity. Therefore, it also explains the previous experimental studies on MoO_x catalyst, and the octahedral MoO_x with higher defect sites is conducive to the realization of high PO selectivity.

4 | Effect of Fe doped dimer MoO_x on propylene epoxidation

Fe based catalyst is an important part of catalyst research. Fe has a certain magnetism and special electronic arrangement. In different catalysts, adding a small amount of Fe often has a special effect. Therefore, this section mainly studies the effect of Fe doping on the catalytic effect of the catalyst, and the partial oxidation mechanism of propylene on the doped catalyst.

4.1 | Effects of Fe doping on The MoO_x cluster of dimers

Figure 8 shows a schematic diagram of MoO_x structure before and after Fe doping.

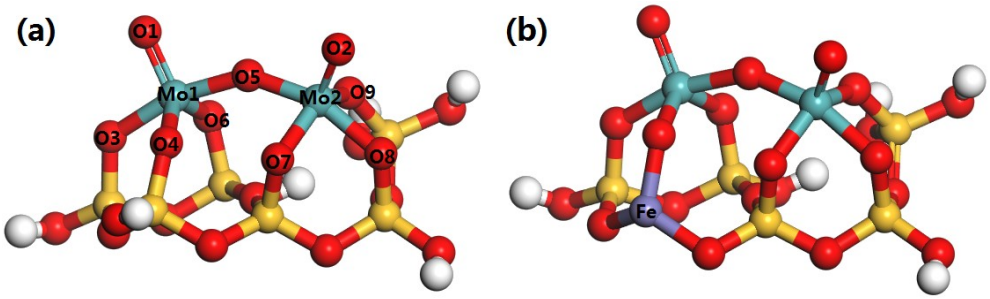

FIGURE 8 Structures diagram of dimer MoO_x before and after Fe doping (the purple ball represents the Fe atom)

It can be seen that the Mo-O bond length and coordination number of MoO_x structure are almost unchanged before and after Fe doping. Moreover, according to Mulliken charge analysis, although the transfer amount is very small, electron transfer mainly occurs on Mo to O3. The number of electrons in the Mo center decreases, and the valence state increases from 1.699 to 1.745, while the O3 valence state decreases from -0.736 to -0.767. It can be seen that the main electron transfer occurs between Fe-O3-Mo, and the addition of Fe makes the electron transfer between Mo-O3 occur, but the charge transfer amount is small.

4.2 | Partial oxidation mechanism of propylene on Fe-doped MoOx cluster

In order to further investigate the effect of Fe doped MoO_x on the partial oxidation of propylene, the AHS process and epoxidation path of C_3H_6 were calculated as shown in Figure 9 and Figure 10, respectively. In the AHS process of C_3H_6 on MoO_x clusters, Mo oh and C_3H_5 are formed after the transition state due to the interaction of Mo=O bond with α-H.

As shown in Figure 9, the energy barrier of this dehydrogenation process is 20.24 kcal/mol, and the energy barrier (45.85 kcal/mol) is greatly reduced (25.61 kcal/mol) compared with that of the undoped system.

As for the formation path of PO on Mo=O bond, compared with the calculated path of undoped system, the difference is that this process is not a direct oxidation process of pulling out O, but also needs to go through an intermediate as shown in Figure 10. Figure 10 (a) shows the epoxidation process on Mo1=O. Mo=O will form Mo-O-C_3H_6 intermediate through the action of C=C bond, and then -C1-O-C2- will form the product PO. Through the analysis of energy diagram, it is found that the energy barrier of Mo1=O for C=C is only 18.49 kcal/mol, while the energy barrier of PO from intermediate to subsequent cyclization is only 6.30 kcal/mol. It is found that the reactivity of Mo=O on MoO_x clusters is much higher than that on MoO_x clusters without Fe doping (energy barrier 45.01 kcal/mol). However, the desorption of PO (19.48 kcal/mol) became the main rate control step. It is difficult to desorb the product, which can easily lead to further reaction or even complete oxidation on the surface.

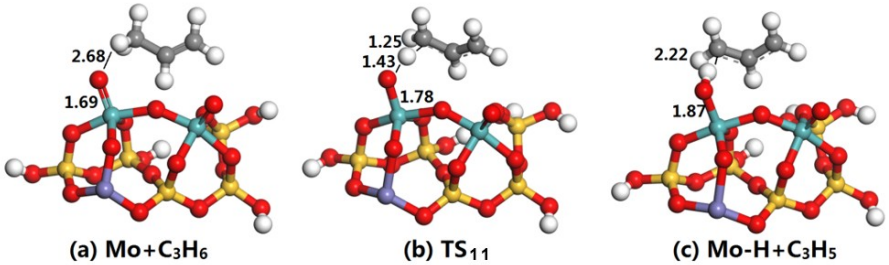

FIGURE 9 AHS process on MoO_x cluster after Fe doping

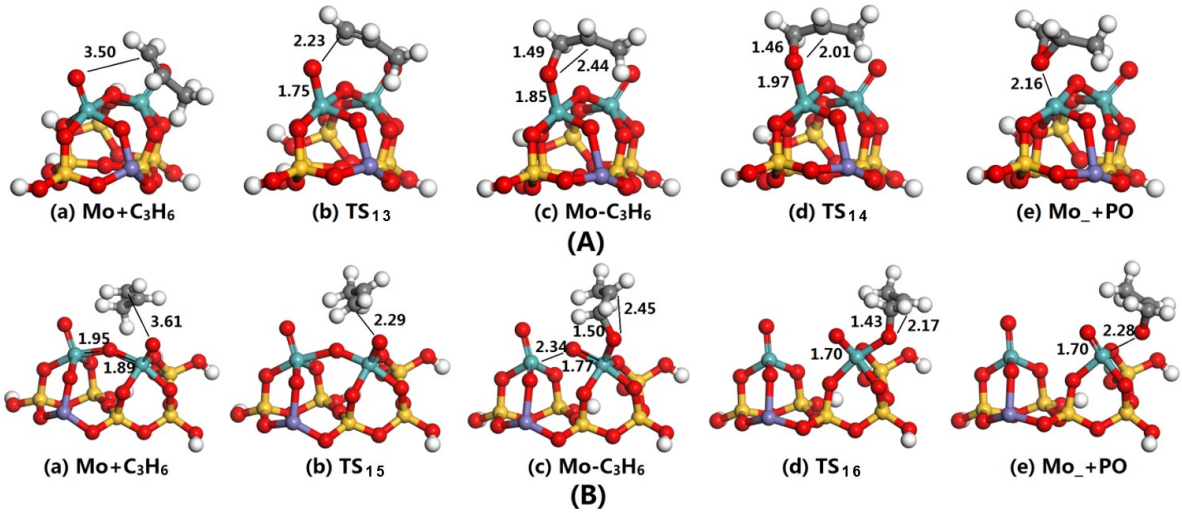

FIGURE 10 PO generation paths on MoO_x cluster after Fe doping: (A) Mo1=O, (B) Mo2=O

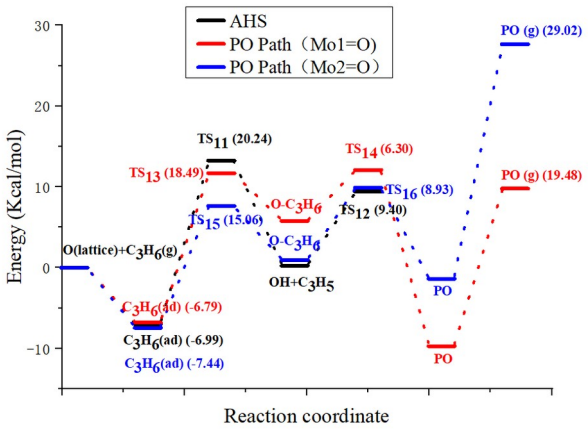

FIGURE 11 Energy profile of different paths of C_3H_6 on MoO_x cluster after Fe doping

The epoxidation of propylene on Mo2=O is similar to that on Mo1=O. Mo2=O first attacks C=C to form intermediate, then the intermediate passes through -C1-O-C2- to form PO. The energy barrier of this process is also not high. The energy barrier of two transition states is 15.06 kcal/mol and 8.93 kcal/mol, and the rate control step is still the desorption of PO (29.02 kcal/mol). However, the spin density analysis shows that the electron arrangement around Fe can hardly affect the far away Mo2 center. Further observation of the whole structure shows that the existence of Fe-O-Mo plays an important role in the stability of MoO_x and its participation in the reaction, because in the undoped MoO_x clusters, it is difficult for propylene to pull O from Mo=O due to the strong bonding of Mo=O bond. However, due to the existence of Fe, the Mo-O bond length between Fe-O-Mo gradually becomes shorter and tends to be the same as that of Mo=O bond during the fracture process of Mo=O double bond. At the same time, the bond cooperation between Fe-O becomes weaker, which weakens the coordination effect of Mo center and makes the process of seizing O easier.

Therefore, the presence of Fe has an important influence on MoO_x clusters, which makes MoO_x clusters have higher reactivity near Mo. By comparing the formation paths of AHS and PO, we can see that the formation path of PO is more

favorable in the former part, but it is difficult for the generated PO to desorb from the system, which may cause further reaction of PO on the surface, which is not favorable for the formation of PO.

4.3 | Influence of Fe doping on defect site formation in MoO_x cluster

The existence of defect sites plays an important influence in propylene epoxidation. In order to further study the effect of Fe on MoO_x, the energy required to form oxygen vacancies in MoO_x configuration before and after Fe doping is listed in Table 3. Figure 12 shows the MoO_x structure with different oxygen vacancies.

TABLE 1 Oxygen vacancy formation energy at MoO_x before and after doped with Fe

Structures	ΔEo (kcal·mol^{-1})	
	O1	O2
Mono-oxo MoO_x	100.10	101.54
Doped with Fe	69.01	100.56
The change	-31.09	-0.98

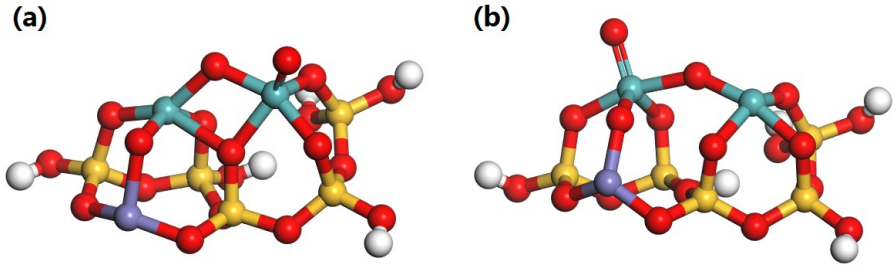

FIGURE 12 Schematic diagram of Fe-doped dimer MoO_x with one O vacancy structure

From the formation energy of defect sites, it can be seen that the oxygen vacancy formation energy near Mo decreases from 100.10 kcal/mol to 69.01 kcal/mol, while the oxygen vacancy formation energy at Mo2 far away from Fe remains unchanged, which indicates that the existence of Fe makes it easier to form defect sites near Mo, and the formation energy decreases greatly. It can be seen from the MoO_x configuration in Figure 12 that the decrease of oxygen vacancy formation energy is closely related to the formation of additional coordination bonds between Mo1 and surrounding O atoms, which makes the structure with defects more stable. From the formation energy of O vacancy, the existence of Fe is beneficial to the formation of defects on MoO_x.

4.4 | Partial oxidation of propylene at Fe-doped MoO_x cluster defect sites

(1) Adsorption of C_3H_6 and O_2 on the defect site

The adsorption configuration of C_3H_6 and O_2 on the defect site is shown in Figure 13. The adsorption of C_3H_6 and O_2 on the defect site is chemical adsorption, forming a bond with Mo center. Among them, C_3H_6 is π-type adsorption, and C=C bond is activated, the bond length is extended from 1.33Å to 1.36Å, and the adsorption energy is -19.11 kcal/mol, which is an exothermic process. The adsorption of O_2 is a stronger exothermic process -52.76 kcal/mol, and the bond length of O_2 is elongated to 1.32 Å, which is similar to that of O_2^-. It can be seen that the existence of defect sites can promote the adsorption of reactant molecules, and the adsorption of O_2 is more favorable. Therefore, the mechanism of O_2 activation will be further analyzed later.

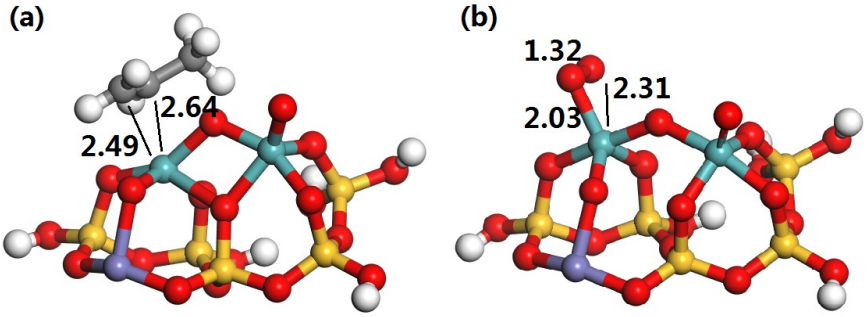

FIGURE 13 The adsorption configuration of C_3H_6 and O_2 at defect site on MoO_x

(2) Partial oxidation of propylene at defect sites

The AHS and epoxidation process of C_3H_6 are mainly studied in the calculation of activation mechanism of O_2. As shown in Figure 14, AHS process mainly involves the capture of α-H by activated O_2 at defect sites. This process is relatively easy to occur, and the energy barrier is only 10.56 kcal/mol, which is equivalent to the desorption energy of 10.80 kcal/mol for C_3H_5.

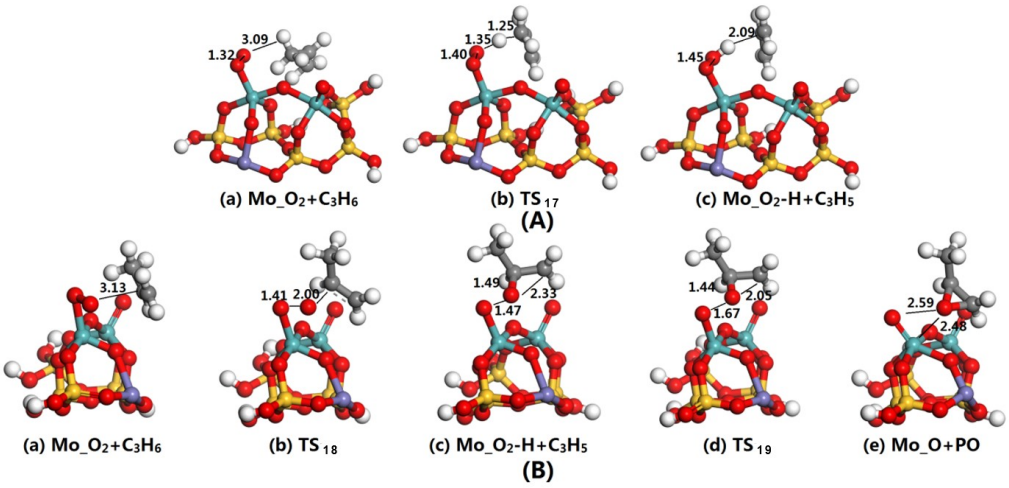

FIGURE 14 Schematic diagram of the AHS process and PO generation path at the defective site

Compared with the reaction process of defect sites on undoped Fe (23.86 kcal/mol), the energy barrier is also greatly reduced. For the formation path of PO, compared with the system without defects, it will pass through a relatively stable intermediate to form PO, which requires 6.63 kcal/mol energy. This is slightly higher than that before Fe doping (3.08 kcal/mol). Similarly, the desorption process of PO is still a rate control step, in which the energy required for the desorption of PO is 11.72 kcal/mol. In contrast, PO generation path with higher exothermic capacity is more likely to occur than AHS process. The energy diagram of AHS process and PO generation path is shown in Figure 15.

Therefore, the main effect of Fe doping is that the energy barrier of dehydrogenation process is reduced. At the same time, compared with the complete MoO_x structure, it is more conducive to the reaction of C_3H_6, and the energy barriers of different paths are lower.

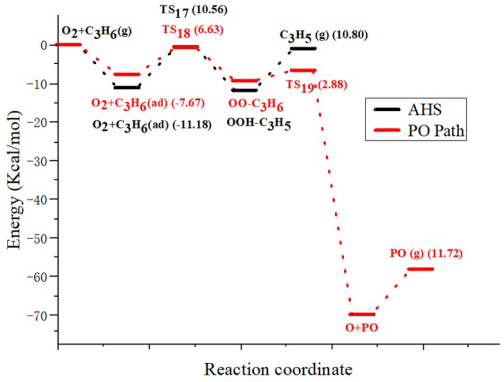

FIGURE 15 Energy diagram of the AHS process and PO generation path at the defect site

5 | Conclusion

In the AHS process, it is found that the O activity in Mo-O-Si is higher, which is beneficial to the AHS process of C_3H_6. Compared with the calculated results of MoO_x of monomer, $Mo(=O)_2$ configuration has higher reactivity. However, there is a high reaction energy barrier for the PO process, which is not conducive to the formation of PO. Therefore, we continue to calculate the MoO_x model of dimer with defect sites, and find that the existence of defect sites in dimer can effectively activate O_2 (O_2^{2-}), and the activated material O has high PO selectivity. Compared with AHS process (energy barrier is 23.86 kcal/mol) and C_3H_5OH process (energy barrier is 15.66 kcal/mol), the energy barrier of PO formation path is very low (energy barrier is 8.9 kcal/mol), and the whole process has high exothermic energy. PO is the main product.

By calculating the different reaction paths (AHS process and PO formation path) of C_3H_6 in the Fe doped coordination dimer MoO_x, it can be seen that Fe doping makes MoO_x clusters more active, and the energy barriers of both AHS process and PO formation path are greatly reduced compared with those before doping. The main problem is that the desorption energy of the product PO is too high, which is not favorable for the selectivity of PO. The existence of Fe makes MoO_x to form defects easily. At the same time, the appearance of defects destroys the equilibrium of MoO_x configuration. The effect of Fe makes the Mo with low coordination easily form coordination bond with the surrounding active O, resulting in the increase of the coordination number of MoO_x from 4 to 5. It is speculated that for the disordered amorphous MoO_x configuration, the effect of Fe is more obvious. The presence of defect sites in dimer can effectively activate O_2 (or O_2). The energy barriers of PO formation reaction (the energy barrier is 11.72 kcal/mol) and AHS process (the energy barrier is 10.80 kcal/mol) on activated O_2 are low. However, the whole process of PO formation has higher heat release, which is more favorable in thermodynamics. Compared with the undoped MoO_x defect sites, the main effect is that the energy barrier of AHS process is greatly reduced. This is not conducive to the selectivity of PO.

Acknowledgements: The author will thank Chen Wei from Wuhan Institute of Physics and Mathematics, Chinese Academy of Sciences for help and encouragement in writing this paper, and also thanks my tutor named Xiaohui Chen and Zhehong Wan for theoretical help in simulation calculation.

ORCID

Xiaohui Chen https://orcid.org/0000-0002-2972-7209

References

1. Russo, V., et al., Chemical and Technical Aspects of Propene Oxide Production via Hydrogen Peroxide (HPPO Process). *Industrial & Engineering Chemistry Research*, **2013**. 52(3): p. 1168-1178.
2. Deshmukh, S., A.V.S. Annaland, and J.A.M. Kuipers, Kinetics of the partial oxidation of methanol over a Fe-Mo catalyst. *Applied Catalysis a-General*, **2005**. 289(2): p. 240-255.
3. Ma, H., et al., Efficient regeneration of Mo/HZSM-5 catalyst by using air with NO in methane dehydro-aromatization reaction. *Applied Catalysis a-General*, **2004**. 275(1-2): p. 183-187.
4. Panov, G.I., et al., Quasi-Catalytic Identification of Intermediates in the Oxidation of Propene to Acrolein over a Multicomponent Bi-Mo Catalyst. *Acs Catalysis*, **2018**. 8(2): p. 1173-1177.
5. Fernandes, C.I., et al., Looking inside the pores of a MCM-41 based Mo heterogeneous styrene oxidation catalyst: an inelastic neutron scattering study. *Physical Chemistry Chemical Physics*, **2016**. 18(26): p. 17272-17280.
6. Getsoian, A.B., V. Shapovalov, and A.T. Bell, DFT plus U Investigation of Propene Oxidation over Bismuth Molybdate: Active Sites, Reaction Intermediates, and the Role of Bismuth. *Journal of Physical Chemistry C*, **2013**. 117(14): p. 7123-7137.
7. Pudar, S., et al., Mechanism of selective oxidation of propene to acrolein on bismuth molybdates from quantum mechanical calculations. *Journal of Physical Chemistry C*, **2007**. 111(44): p. 16405-16415.
8. Song, Z., et al., Gas-phase epoxidation of propylene through radicals generated by silica-supported molybdenum oxide. *Applied Catalysis a-General*, **2007**. 316(2): p. 142-151.
9. Song, Z., et al., Surface-initiated gas-phase epoxidation of propylene with molecular oxygen by silica-supported molybdenum oxide: Effects of addition of C3H8 or NO and reactor design. *Catalysis Letters*, **2008**. 121(1-2): p. 33-38.
10. Sustek, M., et al., Effects of structures of molybdenum catalysts on selectivity in gas-phase propylene oxidation. *Chinese Journal of Catalysis*, **2015**. 36(11): p. 1900-1909.
11. Wan, Z., et al., Theoretical study of propylene epoxidation heterogeneous-homogeneous mechanism overMoO(x)/SiO(2)catalyst. *International Journal of Quantum Chemistry*, **2020**. 120(18).
12. Petersson, G.A., et al., A complete basis set model chemistry .1. the total energies of closed-shell atoms and hydrides of the 1st-row elements. *Journal of Chemical Physics*, **1988**. 89(4): p. 2193-2218.
13. Petersson, G.A. and M.A. Allaham, A complete basis set model chemistry .2. Open-shell systems and the total energies of the 1st-row atoms. *Journal of Chemical Physics*, **1991**. 94(9): p. 6081-6090.
14. P. Hay, T.D.J., Modern theoretical chemistry, Vol. 3. Methods of Electronic Structure Theory. **1976**, *New York: Schaefer III, HF (Ed.) Plenum*.
15. Hay, P.J. and W.R. Wadt, Abinitio effective core potentials for molecular calculations - potentials for the transition-metal atoms Sc to Hg. *Journal of Chemical Physics*, **1985**. 82(1): p. 270-283.
16. Wadt, W.R. and P.J. Hay, Abinitio effective core potentials for molecular calculations - potentials for main group elements Na to Bi. *Journal of*

Chemical Physics, **1985**. 82(1): p. 284-298.

17. Hay, P.J. and W.R. Wadt, Abinitio effective core potentials for molecular calculations - potentials for K to Au including the outermost core orbitals. *Journal of Chemical Physics*, **1985**. 82(1): p. 299-310.
18. M. Francl, W.J.P., W.J. Hehre, et al., Self-consistent molecular orbital methods. XXIII. A polarization-type basis set for second-row elements. *Journal of Chemical Physics*, **1982**. 77 (7): 3654-3665.
19. Spitznagel, G.W., et al., Efficient diffuse function-augmented basis-sets for anion calculation .4. An evaluation of the performance of diffuse function-augmented basis-sets for 2nd-row elements, Na-Cl. *Journal of Computational Chemistry*, **1987**. 8(8): p. 1109-1116.
20. A.D. Mclean, G.S.C., Contracted Gaussian basis sets for molecular calculations. I. Second row atoms, Z=11–18. Journal of Chemical Physics, **1980**. 72 (10): 5639-5648.
21. R. Krishnan, J.S.B., R. Seeger, et al, Self-consistent molecular orbital methods. XX. A basis set for correlated wave functions. *The Journal of chemical physics*, **1980**. 72 (1): 650-654.
22. T. Clark, J.C., G.W. Spitznagel, et al, Efficient diffuse function-augmented basis sets for anion calculations. III. The 3-21+G basis set for first-row elements, Li–F. *Journal of Computational Chemistry*, **1983**. 4 (3): 294-301.
23. Roy, L.E., P.J. Hay, and R.L. Martin, Revised basis sets for the LANL effective core potentials. *Journal of Chemical Theory and Computation*, **2008**. 4(7): p. 1029-1031.